DOI: 10.13009/EUCASS2022-4874

Investigation of Q1D Model for Pressure Oscillations in Solid Rocket Motors

Marco Grossi⋆†, *Daniele Bianchi*⋆ *and Bernardo Favini* ⋆
⋆*Dept. of Mechanical and Aerospace Engineering - Sapienza University of Rome*
Via Eudossiana 18, 00184 - Rome, Italy
marco.grossi@uniroma1.it · daniele.bianchi@uniroma1.it · bernardo.favini@uniroma1.it
†Corresponding author

Abstract

In this work, a Q1D two-phase model developed to analyze pressure oscillations within solid rocket motors is considered. Both vortex-shedding issues and aluminum unsteady combustion are taken into account. In order to investigate the role of each instability source, the Vega P80 motor is taken into account. The experimental P80 SRM PO envelopes are recovered with good correlation, showing the capability of the model to represent the whole PO scenario and highlighting the possible role of aluminum combustion as the root cause for PO dispersion.

1. Introduction

Solid Rocket Motors (SRMs) are known to develop Pressure Oscillations (PO) during their quasi-steady state phase [1]. Since even small pressure oscillations in the combustion chamber are actually able to provide high thrust fluctuations [2, 3], PO risk assessment is actually a mandatory task to be performed during the design process in order to develop a safe and well controlled motor configuration.

In the scientific literature, two physical phenomena are considered to be the major driving mechanisms for PO onset in SRMs used for space launchers [1, 4]: hydrodynamic instabilities related to vortex shedding [5, 6] and thermoacoustic instabilities due to aluminum distributed combustion [7]. Hydrodynamic instabilities involve vortical structures generation and dynamics which lock in with chamber acoustics, giving rise to an aeroacoustic feedback loop. Vortex shedding may occur in a solid rocket chamber due to three different sources: Obstacle Vortex-Shedding (OVS), due to the presence of obstacles to the flow motion along the grain wall as inhibitors or slots; Angular Vortex-Shedding (AVS), caused by sharp discontinuities in the chamber geometry; Parietal Vortex-Shedding (PVS), triggered by a marked motor slenderness able to sustain the Taylor-Culick flow intrinsic instability. Recently, also thermoacoustic instability driven by aluminum unsteady combustion has been numbered as a PO source [7]. Modern solid propellants contain aluminum particles, whose injection in the combustion chamber gives rise to a multiphase reacting flow. Experimental analysis carried out on aluminum combustion have shown that, once the particles are freed from the grain, a certain amount tend to cluster providing agglomerates whose diffusive chemical reaction is strongly influenced by the environment flow condition [8]. As a consequence, a coupling may actually arise if mass and heat release fluctuations produced by the burning droplets are synchronized with the acoustic field [9].

Several approaches are currently employed to investigate PO within SRMs. Static firing tests of real motors and their mock-ups represent the last step in the long-lasting design phase characterized by studies and analyses carried out via numerical tools. Referring to this category, two different methodologies are usually considered: analytical and semi-empirical methods or computational fluid dynamics (CFD) simulations. Unfortunately, both these approaches present some limitations: the formers are conceived to only provide a general estimate of the motor stability behavior regarding specific PO sources; whereas CFD computations are quite costly and delicate since the need of addressing a very rich physical phenomenology ranging from multiphase flows to laminar-turbulence transition. In this context, Q1D methods provide an effective alternative: they are hugely lighter than CFD and, once got over the modeling difficulties, may be able to deliver more details than analytical methods.

The aim of this paper is therefore to investigate and discuss a recently developed and validated Q1D model named TAHR (ThermoAcoustic and Hydrodynamic Resonance) [10]. In next sections TAHR physical and mathematical approaches are described together with numerical results useful to better characterize the model capacity to deal with hydrodynamic and thermoacoustic instabilities.

DOI: 10.13009/EUCASS2022-4874

2. Q1D Mathematical Model

TAHR is a two-phase Q1D model able to compute the internal ballistics of solid motors during their whole operative time together with the major unsteady phenomena able to trigger the onset of pressure oscillations. The models devoted to solving the aeroacoustic and thermoacoustic feedback loops are employed following a particular strategy, based upon the spatial description of the vorticity flowfield:

- In zones devoid of any vortex, as close to the motor head-end, the thermoacoustic model is set on since the presence of a well-organized acoustic boundary layer [11, 12], a paramount flow feature, which plays a key-role in this kind of coupling [7].
- Within regions characterized by the presence of vorticity coherent structures, as in the motor aft, the aeroacoustic model is enforced to simulate and capture vortex-shedding phenomena.

It is worth noticing that, for a given simulation, the code user is responsible for choosing which models to employ and how to set them, therefore a deep and preliminary investigation of the test case under analysis is a mandatory step to ensure reasonable and physically acceptable results.

From a mathematical point of view, TAHR is a Q1D formulation where both gaseous and condensed phase sets of equations are solved by employing a two-way coupling. As for the particles, a pressure-less fully Eulerian model is exploited, with condensed phase supposed dilute (volume fraction $\alpha_p = \frac{\rho_p}{\rho_{Al}} \ll 1$), monodisperse (i.e., a single class of injected particles) and spherical. The governing equations read:

$$\frac{\partial}{\partial t}\begin{pmatrix} U_g \\ U_p \end{pmatrix} + \nabla \begin{pmatrix} F_g \\ F_p \end{pmatrix} = \begin{pmatrix} S_g \\ S_p \end{pmatrix} \tag{1}$$

where U denotes the conservative variable vector, F is the flux vector, and S is the source term vector comprehensive of two-way coupling. Subscripts g and p stand for the gas phase and particle phase, respectively. In launchers solid motor systems, aluminum combustion occurs in a very thin region close to the propellant surface. That is also true for agglomerated particles [13, 14] whose reaction provides products characterized by two different sizes: aluminum oxide smoke and large alumina particles. In the TAHR model, a peculiar modus-operandi is enforced to deal with the several particles present in the flowfield. Since their very localized reaction, burning aluminum agglomerates are not addressed, whereas their effect on the gas phase is considered via combustion source terms. Large inert oxide products are tracked by means of the Q1D approach. Finally, alumina smoke is taken into account directly in the gaseous phase. Via such assumptions, the equations terms for condensed and gaseous phase are so defined:

$$U_p = A\begin{pmatrix} \rho_p \\ \rho_p u_p \\ \rho_p e_p \end{pmatrix} \quad , \quad F_p = A\begin{pmatrix} \rho_p u_p \\ \rho_p u_p^2 \\ \rho_p u_p e_p \end{pmatrix} \quad , \quad S_p = A\begin{pmatrix} \dot{m}_{p,inj} + \dot{m}_{p,cav} \\ F_d \\ H_{p,inj} + H_{p,cav} + F_d u_p + Q_c \end{pmatrix} \tag{2}$$

$$U_g = A\begin{pmatrix} \rho_g \\ \rho_g u_g \\ \rho_g e_g \end{pmatrix} \quad , \quad F_g = A\begin{pmatrix} \rho_g u_g \\ \rho_g u_g^2 + p \\ \rho_g u_g h_g \end{pmatrix} \quad , \quad S_g = A\begin{pmatrix} \dot{m}_{g,inj} + \dot{m}_{g,cav} + \dot{\omega}_p \\ -F_d + S_a^q \\ H_{g,inj} + H_{g,cav} + \dot{\omega}_p Q_{Al} - F_d u_p - Q_c + S_a^e \end{pmatrix} \tag{3}$$

where A represents the motor port area, ρ is the density, u is the velocity and e the total energy. It is worth to be noted that, since only inert particles dynamics is actually evaluated, a fixed particle diameter D_r, given by agglomerates residuals dimension, is imposed. Eq.1 represents an hyperbolic system of Partial Differential Equations (PDE), characterized by strongly non-linear source terms which can be ascribed to the presence of different sub-models. Source terms $(\cdot)_{inj}$ represent mass and energy addition due the propellant grain combustion for gaseous phase and injection of inert particles, whereas $\dot{\omega}_p$ and $\dot{\omega}_p Q_{Al}$ address aluminum combustion sources. Terms $(\cdot)_{cav}$ address mass and energy exchange between the so called "cavity regions", *e.g.* slots, floaters or submerged volume due to the presence of a submerged nozzle, and the bore chamber. Indeed, according to Q1D representation, cavity regions can not be accounted in the mean cross section area, therefore a dedicated sub-model is needed. Two-way coupling between gas and alumina droplets are taken into account thanks to drag force, F_d, and convection heat, Q_c. Finally S_a terms describe gas acoustic field excitation by vortex dynamics. Expressions for drag force and heat transfer are reported in Ref.[15].

2.1 Vortex-Shedding Modeling

In a Q1D fashion, vorticity is naturally neglected in the Euler set of equations, however describing its dynamics is possible thanks to a reduced vorticity equation formally derived from the multi-dimensional one introducing the as-

DOI: 10.13009/EUCASS2022-4874

sumptions of axisymmetric flow [16]:

$$\frac{\partial (\omega A)}{\partial t} + \frac{\partial (k_u u \omega A)}{\partial x} = s_\omega \tag{4}$$

Such equation is coupled and solved along with Eq.1 and represents the main component of the aeroacoustic model. Focusing on Eq.4, two closure terms are added to the standard Q1D equation for vorticity dynamics: s_ω and k_u. The first represents the instantaneous vortex source enabled where vortices are shed in the flow (points like protruding inhibitors or grain angles), whereas the second one is a calibration coefficient acting on the vortex advection velocity and necessary to account for any discrepancy between Q1D and multidimensional vortex velocity. In order to complete the aeroacoustic model, in accordance with the Lighthill-Powell-Howe vortex-sound theory [17], acoustic emissions are provided by the misalignment between acoustic and vortices velocity vectors. Such excitement is introduced thanks to S_a terms in the gaseous phase balance equations. Closure terms description is fully explained and analyzed in previous works [18].

2.2 Aluminum Combustion Modeling

Source terms due to aluminum combustion are built starting from a classical D^2 law and assuming that the reaction products are supposed to be chemically equal to the environment. Mass combustion rate reads:

$$\dot{\omega}_p = 2\pi D n_p \log(1 + B) Sh \tag{5}$$

with B representing the Spalding number, Sh the Sherwood one, n_p the number of particles per unit volume, and D a mean droplet diameter based upon initial agglomerate size, D_i, and oxide residue dimension, D_r. Flow convection effects, extremely important in order to recover any combustion unsteadiness, are taken into account thanks to the Ranz-Marshall correlation [19] which makes use of the particle Reynolds number for the definition of Sh:

$$Sh = (1 + 0.3\, Re_p^{0.5} Pr^{0.33}) \tag{6}$$

$$Re_p = \frac{\rho_g |u_g - u_p| D}{\mu} \tag{7}$$

Particular care must be taken when evaluating Eq.7, since computed Q1D velocities may actually be very different from the one found in a real scenario. That is especially true for velocity oscillating behaviour: the unsteady flowfield of solid motors is characterized by the presence of the acoustic boundary layer, the region close to the propellant grain presenting a layered structure of velocity oscillations [11]. The acoustic boundary layer can not be directly recovered by means of a Q1D method, therefore an additional modeling effort is required in order to properly describe the unsteady combustion of aluminum particles. In the present model, the agglomerates dynamics is evaluated by solving a further equation that describes particles velocity oscillations in the acoustic boundary layer:

$$\frac{\partial u'_p}{\partial t} = \frac{u'_g(1 - F) - u'_p}{\tau_v k_\tau} \tag{8}$$

whereas the term $(1 - F)$ arises from the linearization of the acoustic boundary layer velocity field and acts as a correction for the axial velocity oscillation [7] and k_τ is a calibration parameter necessary to account for the intrinsic acoustic boundary layer multi-dimension. It is important to point out that the F function is evaluated exploiting the combustion zone thickness, in turn estimated via the agglomerates combustion time, a quantity function of D_i and D_r.

3. Pressure Oscillations in Vega P80 SRM

In order to investigate the TAHR model behavior, Q1D simulations have been peformed on the P80 SRM, first stage of the Vega launch vehicle. The P80 motor is characterized by a monolithic aft-finocyl grain design and a composite alluminized propellant, as current practice in every European solid rocket motor of latest generation.

Non-dimensional PO envelops, obtained from the first eleven Vega flights, are reported in Fig.1. As it is possible to observe, PO show a decreasing trend over time and a flickering behavior that breaks down the overall signature in four distinct blows. One of the most striking features visible in the experimental dataset is the strong dispersion influencing both amplitude and time windows of occurrence. The origin of such behavior is not clear, however some evidence allows to draw preliminary conclusions. Contrary to pressure oscillations envelopes, mean pressure curves exhibit a strong repetitiveness among the flights, suggesting that propellant grain geometry and other ballistic properties are essentially the same. In light of this, it is reasonable to suppose that the root cause of PO dispersion is related to

DOI: 10.13009/EUCASS2022-4874

the combustion processes occurring at the propellant surface and, specifically, to the effect of the aluminum distributed combustion. Thermoacoustic instability level is deeply affected by aluminum agglomerates amount and dimension, features strictly related to propellant composition and granulometry which, in turn, can undergo slight modifications from one flight to another.

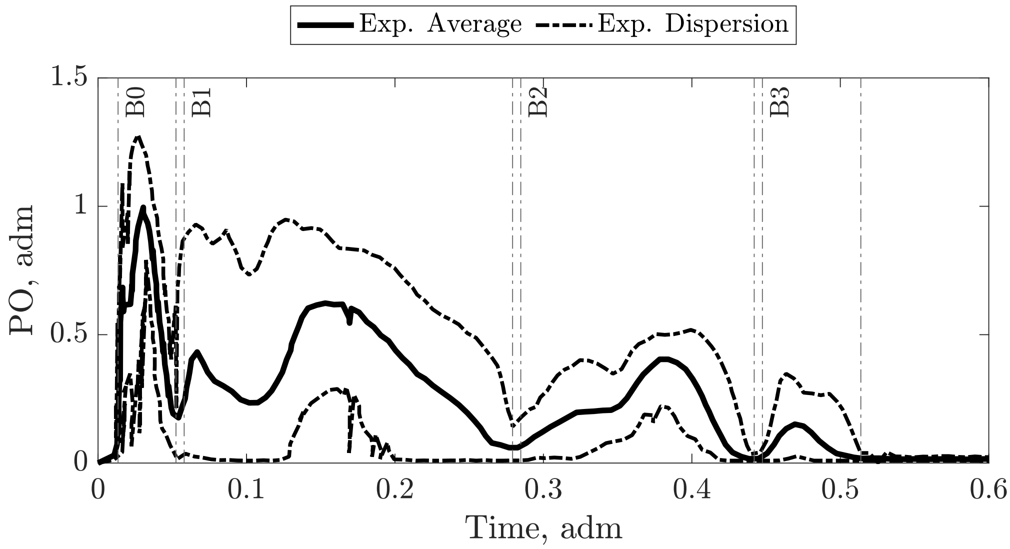

Figure 1: P80 SRM pressure oscillations.

3.1 Source Identification

Several methodologies may be applied in order to identify the driving mechanism behind pressure oscillations onset in a specific SRM. However, when experimental data are available, analytical and semi-empirical methods have proved to be quite reliant to accomplish such task [20]. For such reason, a preliminary risk assessment of P80 PO is carried out exploiting a set of tools presented in the scientific literature over the years. All the necessary quantities (*e.g.* mean flow velocity and geometry evolution over time) are evaluated thanks to an in-house ballistic solver.

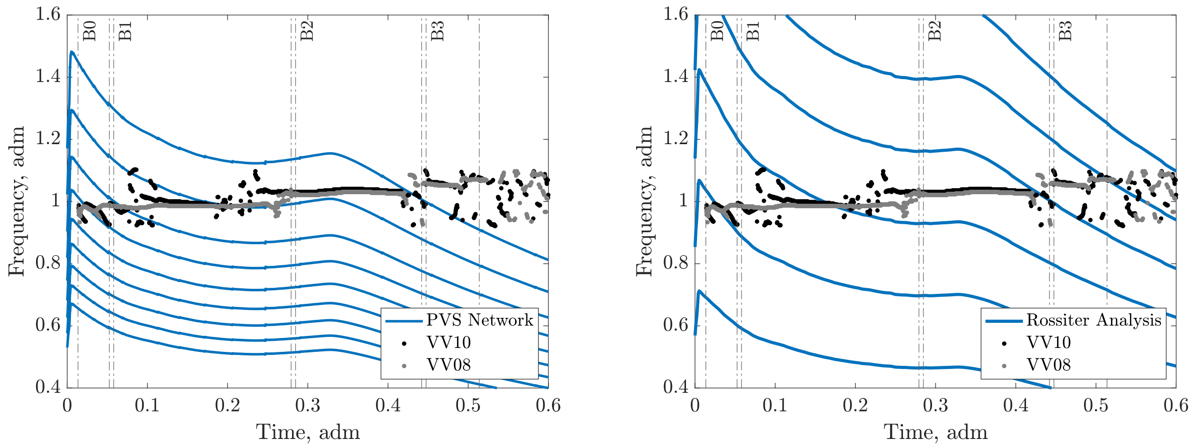

(a) PVS: Biglobal linear stability analysis.

(b) AVS: Rossiter analysis.

Figure 2: Hydrodynamic instabilities in P80 SRM.

Since the monolithic design of the P80 motor, PVS and AVS are the only kind of hydrodynamic instabilities that can develop. The PVS risk assessment is achieved thanks to the biglobal linear stability analysis firstly developed by Chedevergne *et al.* [21]. The same circular frequencies used in Refs.[22, 23] are assumed to build the vortex-shedding frequency network. On the other hand, the Rossiter semi-empirical formula [24] is solved to assess AVS,

DOI: 10.13009/EUCASS2022-4874

employing the same parameters exploited in Ref.[25]. Fig.2 provides a comparison between PVS (see Fig.2a) and AVS (see Fig.2b) frequencies and pressure instability frequency data extracted from two Vega flights. Accordingly with the flute-mode theory, instability phenomena reliant on hydrodynamic instabilities exhibit a typical frequency behavior characterized by the following of PVS or AVS patterns alternate with frequency jumps when those patterns are too far from the motor acoustic frequency [5]. As a matter of fact, experimental patterns faithfully follow hydrodynamic frequencies only in the B0 time window, whereas, after such phase, flights data show up a very different behavior compared with the computed frequencies, suggesting that hydrodynamic instabilities are not the major responsible for pressure oscillations onset after B0.

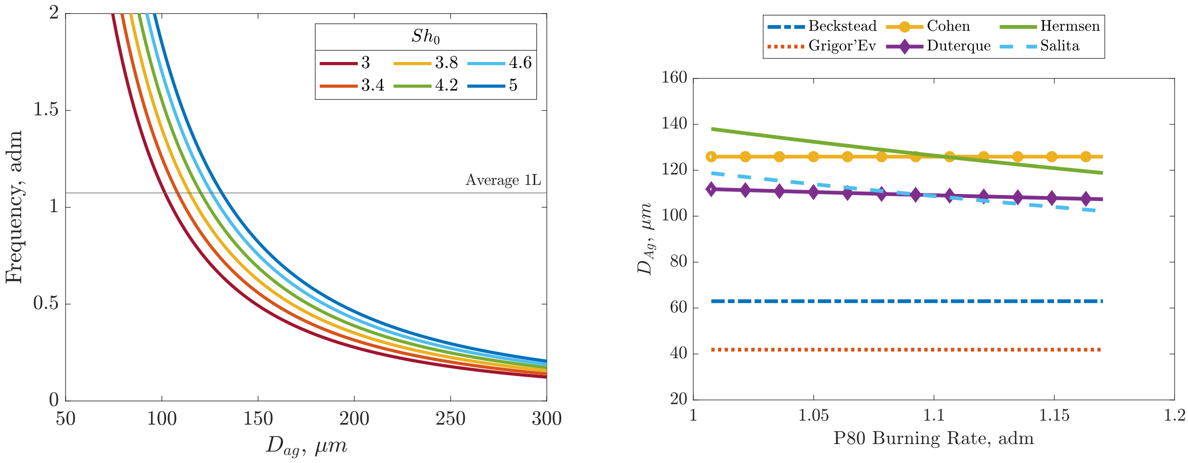

(a) Instability frequencies.

(b) Aluminum agglomerates diameter prediction.

Figure 3: Thermoacoustic instability risk assessment in P80 SRM.

The possible presence of thermoacoustic instability is investigated through the 'rule of thumb' proposed by Gallier and Godfroy [7]. This approach provides the frequency which, assuming a certain set of aluminum droplets size and dynamics, a SRM flowfield should present to be more excited by thermoacoustic phenomena. The outcomes are pictured in Fig.3a. As it is clearly evident, the maximum excited frequencies due to thermoacoustic instability match the motor first acoustic frequency for agglomerate size in the approximate range 100 to 150 μm. It is important to note that a SRM could be unstable even if particles properties and flow dynamics do not ensure a perfect match between the motor acoustic frequency and the ones linked to maximum excitation [7]. In order to complete the present analysis, it would be useful to have a good estimate of the aluminum agglomerate size generated by the P80 propellant. Unfortunately, such information is not easy to provide: propellant composition, in terms of ingredients granulometry, is not fully known and might vary from one flight to another; moreover, mathematical models, currently present in the state of the art, furnish a large data scattering when it comes to predicting aluminum agglomerates size. In this scenario, both experimental data and the application of mathematical models may help. Concerning the first category, lab-scale experiments run on propellant formulations very similar to the P80 one, in terms of components proportions, actually yield agglomerate size compliant with the aforementioned unstable range ([26, 27]). The same conclusion may be drawn by exploiting the mathematical models. In Fig.3b, aluminum agglomerates diameter is evaluated as function of P80 burning rate. As it is possible to see, the majority of the models collocates the predicted agglomerates diameter within the range related to a thermoacoustic coupling, confirming the possibility to have such an issue in the P80 motor during the whole operative time.

3.2 Q1D Simulations

The first step needed to perform TAHR computations consists of the model setup. In this spirit, the outcomes presented in Sec.3.1 play a paramount role since, suggesting the potential presence of hydrodynamic and thermoacoustic instabilities, prompt an a priori estimate of the vorticity flowfield evolution. This task is accomplished by analyzing the motor geometry. In Fig.4,the Q1D domain is compared with the 3D configuration of P80 SRM at the initial time. Accordingly to the physical phenomenology of PVS and AVS, vortices generation is likely to occur only in the terminal part of the motor cylinder, leaving space for the acoustic boundary layer development in the volume far upstream of the finned region. As time runs forward, the scenario gradually changes due to the geometry evolution. The recovery

DOI: 10.13009/EUCASS2022-4874

of this behavior is entrusted to the calibration of the vortices velocity and, since the presence of PVS phenomena, to an L/D criterion which limits vortex generation once it reaches a certain threshold.

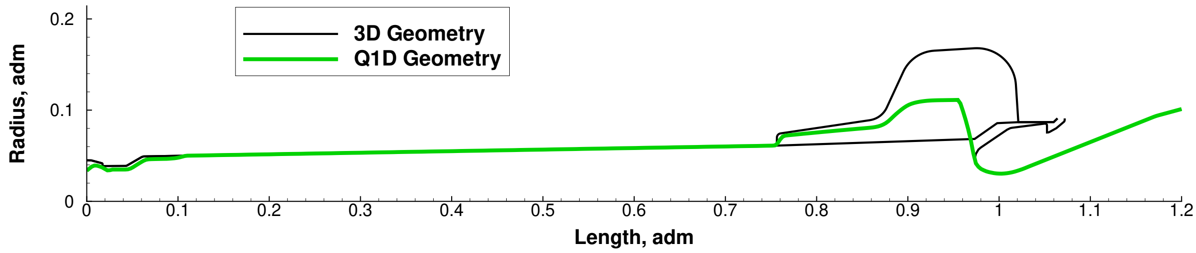

Figure 4: P80 SRM Q1D and 3D geometries at ignition time.

Fundamental input data concern aluminum agglomerates properties, in particular their amount, size and combustion residue dimension. All of these data are unfortunately affected by strong uncertainty. In this work, one third of the overall amount of aluminum is set to agglomerate [26], alumina droplets diameter is considered to be half of the initial agglomerate one [28], which, in turn, is defined accordingly to the results presented in Sec.3.1.

Finally TAHR calibration must be addressed. The model parameter for the vorticity source term and the one for the agglomerates velocity equation are taken from test case simulations used to validate the model [15, 29], whereas the vortices transport calibration arises from a comparison between CFD and Q1D velocity flowfields. Ad-hoc calibrations based upon the experimental data of the motor are therefore avoided.

TAHR Q1D solutions for P80 SRM are shown and compared with the average PO experimental envelope in Fig.5. Three different PO outcomes are reported: a full TAHR solution (green line), a pure hydrodynamic result (blue line), and a thermoacoustic one (red line). The condition $D_i = 140\,\mu m$ is employed for the two-phase computations. Taking into account the TAHR result, a very good agreement is found with the average PO data in terms of amplitude and time windows of occurrence for B0 and B1. On the contrary B2 and B3 are not recovered by the Q1D solution. Despite this discrepancy, it is important to stress the relevance of the obtained result: as a matter of fact, TAHR model is able to recover the two most powerful blows employing a simplified input (constant aluminum properties) given by a propellant analysis and without any change in the model calibration with regard to the validation tests.

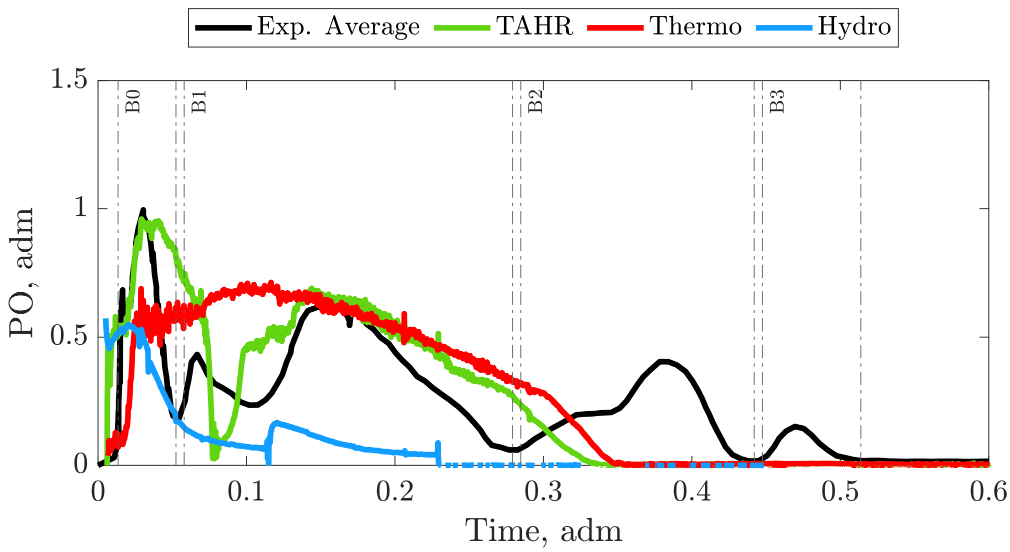

Figure 5: TAHR PO solution for P80 SRM at $D_i = 140\,\mu m$.

Comparing the three Q1D solutions, it is clearly evident that the PO envelope shape provided by the full model results from a sort of superposition of the two separate sources. Indeed, the TAHR outcome has a PO structure very similar to the one obtained with a pure hydrodynamic simulation, since B0 and B1 are neatly represented along with their abrupt separation. On the other hand, the thermoacoustic contribution is clearly evident in the amplitude and in the instability increased lasting. This comparison permits to assess the role of each PO source: hydrodynamics is responsible for blows structure with a primary role in B0; the thermoacoustic coupling due to aluminum combustion deeply

DOI: 10.13009/EUCASS2022-4874

affects both amplitude and blows time of occurrence, with a fundamental contribution for the B1. These conclusions are in agreement with the analysis carried out in Sec.3.1.

The last step in P80 analysis is focused on the study of PO dispersion. The PO dispersion could be caused by the onset of different conditions in the thermoacoustic coupling triggered by tiny modifications of propellant microstructure from one flight to another. In this spirit, several simulations have been performed varying the size of the aluminum agglomerates in the range $130 - 150\,\mu m$. All other model inputs and calibations are kept unchanged.

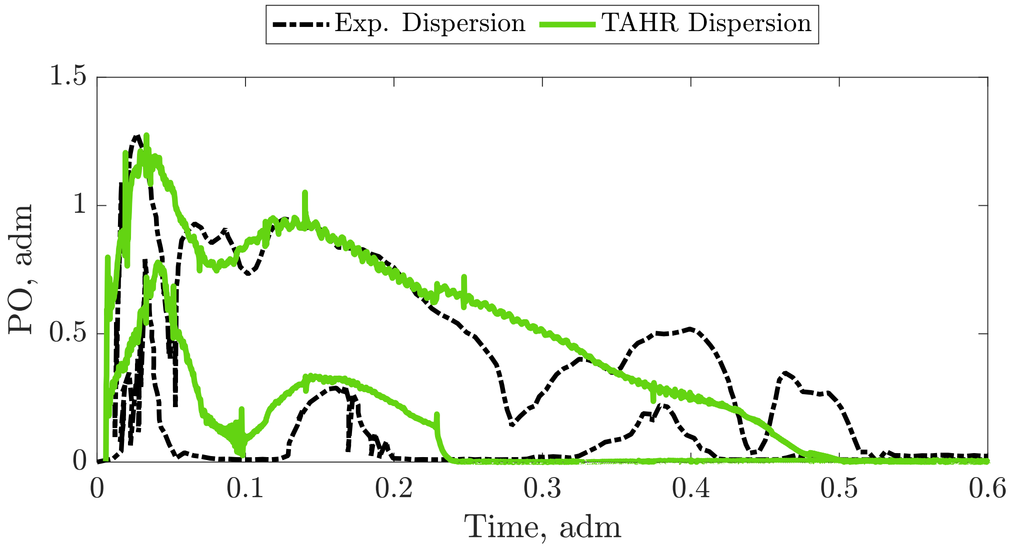

Figure 6: TAHR PO solution for P80 SRM accounting for several agglomerates size ($D_i = 130 - 150\,\mu m$).

In Fig.6 the experimental dispersion envelope is shown together with TAHR numerical solutions. As it is possible to see a very good agreement is found regarding PO amplitude for B0 and B1. The amplitude decreasing tendency is righteously recovered as well as the instability longer lasting associated with the higher pressure oscillations level. These outcomes prove that slight differences of propellant microstructure occurring from one P80 firing to another are a reasonable physical explanation for P80 SRM PO dispersion.

4. Conclusions

This work is dedicated to the investigation of a Q1D two-phase model, named TAHR, focused on pressure oscillations within solid rocket motors. Two kind of phenomena, recognized in the current state of the art as major instabilities in modern solid motors used in launch vehicles, are considered: aeroacoustic feedback loop related to vortex-shedding and thermoacoustic coupling triggered by the aluminum distributed combustion.

In order to investigate the model, the Vega P80 SRM is chosen as reference case. This motor is prone to develop pressure oscillations during the first half of its operative time, and it is affected by large dispersion concerning the pressure oscillations signature. The origins of pressure oscillations have been addressed via a preliminary risk assessment carried out through analytical and semi-empirical tools widely employed in the scientific literature. This study has highlighted the role of vortex-shedding phenomena during the first seconds of the motor functioning and the likely onset of thermoacoustic coupling driven by aluminum distributed combustion throughout the entire unstable time interval.

Subsequently, numerical simulations have been performed using the in-house TAHR model. Experimental data presented in the scientific literature and the application of mathematical models are exploited to define a reasonable aluminum agglomerates size range, whereas the model calibration comes from previously performed validation test cases. The comparison between the P80 SRM PO average signature and the numerical result shows a very good agreement in terms of overall trend, recovering both amplitude and time window of occurrence for the first two blows. This result agrees with the outcomes of the risk assessment analysis, showing that both hydrodynamic and thermoacoustic instabilities are necessary to recover the PO level. Finally, PO dispersion has been put under analysis. Propellant influence on aluminum unsteady combustion has been supposed to be the root cause for the large scattering presented by the experimental data. To simulate such conditions, TAHR computations have been run with different agglomerates diameters. The numerical outcomes confirm the assumptions made, showing a close match between measured and computed PO levels of the P80 motor.

DOI: 10.13009/EUCASS2022-4874

References

[1] F. Culick and P. Kuentzmann, "Unsteady motions in combustion chambers for propulsion systems," tech. rep., NATO Research and Technology Organization Neuilly-Sur-Seine (France), 2006.

[2] Y. Fabignon, J. Dupays, G. Avalon, F. Vuillot, N. Lupoglazoff, G. Casalis, and M. Prévost, "Instabilities and pressure oscillations in solid rocket motors," *Aerospace science and technology*, vol. 7, no. 3, pp. 191–200, 2003.

[3] J. Anthoine, "Solid propellant pressure oscillations," 2014. STO-EN-AVT-206. RTO/NATO.

[4] G. Casalis, G. Boyer, and E. Radenac, "Some recent advances in the instabilities occurring in long Solid Rocket Motors," in *47th AIAA/ASME/SAE/ASEE Joint Propulsion Conference and Exhibit 2011*, 2011.

[5] K. Dotson, S. Koshigoe, and K. Pace, "Vortex shedding in a large solid rocket motor without inhibitors at the segment interfaces," *Journal of Propulsion and Power*, vol. 13, no. 2, pp. 197–206, 1997.

[6] G. A. Flandro and J. Majdalani, "Aeroacoustic instability in rockets," *AIAA journal*, vol. 41, no. 3, pp. 485–497, 2003.

[7] S. Gallier and F. Godfroy, "Aluminum combustion driven instabilities in solid rocket motors," *Journal of propulsion and power*, vol. 25, no. 2, pp. 509–521, 2009.

[8] H. Rezaiguia, P. Liu, and T. Yang, "Flame response of solid propellant AP/Al/HTPB to a longitudinal acoustic wave," *International Journal of Spray and Combustion Dynamics*, vol. 9, no. 4, pp. 241–259, 2017.

[9] S. Gallier, F. Sibe, and O. Orlandi, "Combustion response of an aluminum droplet burning in air," *Proceedings of the Combustion Institute*, vol. 33, no. 2, 2011.

[10] M. Grossi, D. Bianchi, and B. Favini, "Aerothermoacoustics q1d modeling for solid rocket motors instabilities," in *AIAA SciTech 2022 Forum*, p. 1897, 2022.

[11] G. A. Flandro, "Effects of vorticity on rocket combustion stability," *Journal of Propulsion and Power*, vol. 11, july-august 1995.

[12] J. Majdalani and G. A. Flandro, "The oscillatory pipe flow with arbitrary wall injection," *Proceedings of the Royal Society of London. Series A: Mathematical, Physical and Engineering Sciences*, vol. 458, no. 2023, pp. 1621–1651, 2002.

[13] M. Grossi, D. Bianchi, and B. Favini, "Modeling multiphase effects on pressure oscillations in solid propulsion," in *AIAA Propulsion and Energy 2020 Forum*, p. 3927, 2020.

[14] A. Genot, S. Gallier, and T. Schuller, "Model for acoustic induced aluminum combustion fluctuations in solid rocket motors," *Journal of Propulsion and Power*, vol. 35, no. 4, pp. 720–735, 2019.

[15] M. Grossi, D. Bianchi, and B. Favini, "Thermoacoustics q1d modeling in solid rocket motors," in *AIAA Propulsion and Energy 2021 Forum*, 2021.

[16] V. Ferretti, *Numerical simulations of acoustic resonance of Solid Rocket Motor*. PhD thesis, Department of Aerospace and Mechanical Engineering, Sapienza University of Rome, 2011.

[17] M. Howe, *Acoustics of Fluid-Structure Interactions*. New York: Cambridge Univ. Press, 1998.

[18] M. Grossi, M. Laureti, and B. Favini, "Quasi-one dimensional model of pressure oscillations in aft-finocyl solid rocket motors: a critical evaluation of alternative closure sub-models and calibrations," in *AIAA Propulsion and Energy 2019 Forum*, p. 4137, 2019.

[19] W. E. Ranz and W. R. Marshall, "Evaporation from drops," *Chemical Engineering Progress*, vol. 48, no. 3, pp. 141–146, 1952.

[20] J. F. Guéry, S. Ballereau, F. Godfroy, S. Gallier, O. Orlandi, P. Della Pieta, E. Robert, and N. Cesco, "Thrust oscillations in solid rocket motors," in *44th AIAA/ASME/SAE/ASEE Joint Propulsion Conference and Exhibit*, pp. 1–15, 2008.

[21] F. Chedevergne, G. Casalis, and T. Feraille, "Biglobal linear stability analysis of the flow induced by wall injection," *Physics of Fluids*, vol. 18, no. 1, p. 014103, 2006.

DOI: 10.13009/EUCASS2022-4874

[22] F. Chedevergne and G. Casalis, "Detailed analysis of the thrust oscillations in reduced scale solid rocket motors," in *42nd AIAA/ASME/SAE/ASEE Joint Propulsion Conference*, vol. 2, pp. 1047–1058, 2006.

[23] G. Boyer, G. Casalis, and J.-l. Estivalezes, "Theoretical investigation of the parietal vortex shedding in solid rocket motors," in *48th AIAA/ASME/SAE/ASEE Joint Propulsion Conference & Exhibit*, p. 3825, 2012.

[24] J. Rossiter, "Wind-tunnel experiments on the flow over rectangular cavities at subsonic and transonic speeds," *Aeronautical Research Council Reports & Memoranda*, 1964.

[25] K. Dotson, J. Womack, and P. Grosserode, "Structural dynamic analysis of solid rocket motor resonant burning," *Journal of Propulsion and Power*, vol. 17, no. 2, pp. 347–354, 2001.

[26] J. Duterque, "Experimental studies of aluminum agglomeration in solid rocket motors," *International Journal of Energetic Materials and Chemical Propulsion*, vol. 4, no. 1-6, 1997.

[27] F. Maggi, L. T. DeLuca, and A. Bandera, "Pocket model for aluminum agglomeration based on propellant microstructure," *AIAA Journal*, vol. 53, no. 11, pp. 3395–3403, 2015.

[28] M. Salita, "Survey of recent Al2O3 droplet size data in solid rocket chambers, nozzles, and plumes," in *21st JANNAF Exhaust Plume Technology Meeting*, vol. 1, p. 1, Oct. 1994.

[29] M. Grossi, D. Bianchi, and B. Favini, "Q1d modeling of hydrodynamic instabilities in solid rocket motors," in *Mathematical Problems in Aerospace Science Symposium*, 2021.